Environmental Pollution 268 (2021) 115780

Contents lists available at ScienceDirect

Environmental Pollution

journal homepage: www.elsevier.com/locate/envpol

Seasonal variations in the mass characteristics and optical properties of carbonaceous constituents of $PM_{2.5}$ in six cities of North China☆

Lining Luo [a, b], Hezhong Tian [a, b, *], Huanjia Liu [a, b], Xiaoxuan Bai [a, b], Wei Liu [a, b], Shuhan Liu [a, b], Bobo Wu [a, b], Shumin Lin [a, b], Shuang Zhao [a, b], Yan Hao [a, b], Yujiao Sun [c], Jiming Hao [d], Kai Zhang [e]

[a] State Key Laboratory of Environmental Simulation and Pollution Control, School of Environment, Beijing Normal University, Beijing, 100875, China
[b] Center for Atmospheric Environmental Studies, Beijing Normal University, Beijing, 100875, China
[c] College of Water Sciences, Beijing Normal University, Beijing, 100875, China
[d] School of Environment, Tsinghua University, Beijing, 100084, China
[e] Department of Epidemiology, Human Genetics and Environmental Sciences, The University of Texas Health Science Center at Houston School of Public Health, Houston, TX, 77030, USA

ARTICLE INFO

Article history:
Received 9 March 2020
Received in revised form
1 October 2020
Accepted 4 October 2020
Available online 20 October 2020

Keywords:
Carbonaceous constituents
brown carbon
OC/EC
$PM_{2.5}$
Light-absorption properties
North China

ABSTRACT

Carbonaceous constituents have various adverse impacts on human health, visibility, and climate change. Although comprehensive studies on the characteristics of carbonaceous constituents have been conducted recently, systematic studies covering both the mass characteristics and light-absorption properties of carbonaceous constituents on a regional scale in China are quite limited. In this study, current seasonal measurements of organic carbon (OC) and elemental carbon (EC) in $PM_{2.5}$ were investigated during autumn and winter (1–30 October 2017 and December 18, 2017 to January 17, 2018) in six selected cities located at the eastern foot of the Taihang Mountains: Beijing, Baoding, Shijiazhuang, Handan, Xinxiang, and Zhengzhou. Seasonal variations were similar when Beijing was excluded. The lowest concentrations of OC (18.33 ± 9.39 μg/m^3) and EC (7.66 ± 5.64 μg/m^3) were observed in Xinxiang (autumn) and Beijing (winter), respectively, while the highest concentrations of OC (38.43 ± 62.10 μg/m^3) and EC (12.24 ± 24.67 μg/m^3) occurred in Baoding during winter mainly due to elevated fuel combustion for space heating. The results of the potential source contribution function (PSCF) analysis suggested that border zones between several provinces in North China should be highlighted in order to strengthen pollution control. Moreover, by separating the optical properties of brown carbon from those of black carbon, we were able to estimate the contributions of brown carbon to the $PM_{2.5}$ total light-absorption coefficient. The results show that the brown carbon absorption coefficient (at 405 nm) in winter at six sites accounted for 21.2%, 33.3%, 34.7%, 39.1%, 48.6%, and 23.3% of the $PM_{2.5}$ light absorption, which are values that are comparable to the contribution of black carbon in Xinxiang. These results provide a more comprehensive understanding of carbonaceous constituents on a regional scale.

Author contributions

Lining Luo and Hezhong Tian contributed to Conceptualization, Methodology, Software, Writing-Original Draft, Writing-Reviewing and Editing. Lining Luo, Huanjia Liu, Xiaoxuan Bai, Wei Liu, Shuhan Liu, Bobo Wu, Shumin Lin, Shuang Zhao, Yan Hao, Yujiao Sun, and Kai Zhang contributed to field tests and samples analysis. Hezhong Tian and Jiming Hao contributed to reviewing the manuscript and critically revising the draft. We certify that our manuscript is original research, it has not been previously published and submitted for publication elsewhere in identical or similar form, nor it will be while it is under consideration in Environmental Pollution. Finally, all the authors declare that there is not any conflict of interest regarding the material discussed in the manuscript.

☆ This paper has been recommended for acceptance by Admir C. Targino.

* Corresponding author. State Key Laboratory of Environmental Simulation and Pollution Control, School of Environment, Beijing Normal University, Beijing, 100875, China.
E-mail address: hztian@bnu.edu.cn (H. Tian).

https://doi.org/10.1016/j.envpol.2020.115780
0269-7491/

1. Introduction

Many megacities and city-cluster regions in the world have been confronting severe air pollution, which causes approximately 4.2 million premature deaths annually (WHO, 2018). As a result of a rapidly developing economy and the acceleration of urbanization, anthropogenic activities have led to severe air pollution in China (Li et al., 2019; Tian et al., 2011). Specifically, heavy haze pollution in large areas of North China in January 2013 attracted worldwide attention and triggered the implementation of the Blue Sky Defense initiative by the Chinese government. To mitigate severe air pollution, the Air Pollution Prevention and Control Action Plan (APPCAP) was promulgated by the Ministry of Ecological Environmental Protection (MEE) in September 2013; however, severe pollution episodes still frequently occur in the Beijing-Tian-Hebei region (BTH) and its surrounding provinces. It has been acknowledged that $PM_{2.5}$ (particulate matter with an aerodynamic diameter less than 2.5 μm) plays an important role in human health risks (Wiedensohler et al., 2009; Galvao et al., 2018; Araki et al., 2020) and climate change; in particular, organic carbon (OC) and elemental carbon (EC) directly scatter and absorb solar radiation and can contribute to direct aerosol climate effects (Bond et al., 2013; Sarkar et al., 2019; Mbengue et al., 2020). Previous studies have provided evidence that certain aerosol-radiation interactions tend to cool or heat the earth's surface, increasing atmospheric stability, and enhancing the accumulation and formation of particulate matter, eventually decreasing air quality (Wu et al., 2020; Petaja et al., 2016).

Significant decreases in $PM_{2.5}$ concentrations were found in the BTH region (from 106 to 64 μg/m^3 during 2013–2017), while $PM_{2.5}$ concentrations in the BTH region remained 1.45–1.88 times higher than in the Yangtze River Delta (YRD) and Pearl River Delta (PRD) regions especially in autumn and winter, respectively (Ding et al., 2019; Zhao et al., 2015). The BTH region is still one of the most polluted areas in China due to high emissions from the consumption of fossil fuels and bioenergy, which are the main sources of OC and EC. Many scientists have conducted research on apportioning the spatiotemporal characteristics and source origins of OC and EC. Zhao et al. (2013) reported a decrease in EC concentrations due to a reduction in coal consumption. Ji et al. (2019) presented the variation characteristics of carbonaceous constituents in Beijing during 2013–2017 under air pollution control measures. Online measurements conducted in the BTH region indicated that carbonaceous constituent levels remained serious; however, the environmental effects caused by carbonaceous aerosols are related to not only their mass concentrations, but also their optical properties.

Generally, carbonaceous constituents are operationally divided into OC and EC, respectively (Andreae and Gelencs'er, 2006; Yttri et al., 2019). Black carbon (BC) is considered one of the most important factors influencing global warming (Bond et al., 2013; Koch et al., 2007), with previous studies indicating that BC could warm the atmosphere by absorbing solar radiation; in contrast, organic carbon only cools the atmosphere by scattering (Koch et al., 2007). However, the effects of organic carbon on light absorption are poorly understood. Most models that simulate aerosol radiative forcing treated organic carbon as scattering particles that only cool the atmosphere, neglecting the absorption of solar radiation (Bahadur et al., 2012; Menon et al., 2002). Recent studies have revealed that brown carbon (BrC) is mainly emitted by biomass burning (Tian et al., 2019) and fossil fuel combustion (Yan et al., 2017), and it exhibits a strong absorption in the near-ultraviolet-visible spectrum range (Feng et al., 2013).

Previous studies on the light absorption of carbonaceous aerosols, especially on BrC, have mostly focused on megacities or specific areas. Cheng et al. (2016) revealed that the absorption of BrC in Beijing during the winter could be comparable to that of BC in the UV spectrum range. Xie et al. (2019) reported that BrC in Beijing during the winter accounted for 46% and 48% of the total absorption at 307 nm at ground level and at 260 m, respectively. Zhao et al. (2019) indicated that BrC accounted for 44% of the total light absorption at 405 nm in the Tibetan Plateau. Previous studies have also demonstrated that BrC contributed 12–15% of the measured absorption at 405 nm during the summer and 15–19% during the autumn in Guangzhou (Lei et al., 2019).

In this study, OC and EC in $PM_{2.5}$ were collected at six sites-Beijing (BJ), Baoding (BD), Shijiazhuang (SJZ), Handan (HD), Xinxiang (XX), and Zhengzhou (ZZ)-representing several highly polluted cities alongside the eastern foot of the Taihang Mountains. Seasonal variations in carbonaceous constituents, as well as their light absorption properties were investigated. Moreover, we calculated the contribution of BrC to the total $PM_{2.5}$ light absorption at a regional scale. The results of this study provide significant implications for evaluating the effects of carbonaceous aerosols on human health and better estimate the effects of carbonaceous aerosol light absorption on climate change at a regional scale.

2. Methodology and data sources

2.1. Field sampling and measurements

Ambient $PM_{2.5}$ was collected at six cities during the selected study period (1–30 October 2017 and December 18, 2017 to January 17, 2018), which represents the autumn and winter seasons, respectively. The six cities considered are all located alongside the eastern foot of the Taihang Mountains, as shown in Fig. 1, with more details outlined in Table S1.

Daily $PM_{2.5}$ samples were collected on quartz filters (Pallflex Tissuquartz™, 90 mm, USA) for 23 h (from 9:00 a.m. to 8:00 a.m.) per day at the six sampling points with TH-150C medium volume samplers (Wuhan Tianhong Instruments Co., Ltd., flow rate: 100 L/min). In total, 366 samples were obtained, and all procedures were strictly quality controlled. More details on the sampling collection procedure are provided in previous study (Liu et al., 2019a).

2.2. Experiments

Before sampling, all the quartz filters were placed in a furnace wrapped in aluminum foil at 450 °C for 4 h to remove residual organic components. They were then placed in a desiccator at a constant temperature (25 °C) and humidity (50%) for 48 h before weighing. The difference in the weights before and after sampling was recorded as the mass concentration of the collected $PM_{2.5}$. The filters were then placed at −20 °C until further analysis.

2.3. Carbonaceous components analysis

IMPROVE and NIOSH are two frequent protocols for the measurement of OC and EC, which use differing temperature ramping, step duration and optical correction schemes (Cavalli et al., 2010; Wu et al., 2016). More details on the different protocols and limitations are discussed in the supplementary material. In this study, we selected DRI-2015 with IMPROVE_A for the measurement of OC and EC. An area of 0.532 cm^2 from each filter was placed in an oven to analyze the eight carbon fractions. The nominal temperature plateaus in 100% He are 120 °C, 250 °C, 450 °C, and 550 °C, and the corresponding thermal carbon fractions are called *OC1*, *OC2*, *OC3*, and *OC4*, respectively. The nominal temperature plateaus in the 98% He/2% O_2 atmosphere are 550 °C (*EC1*), 700 °C (*EC2*), and 800 °C (*EC3*). OC=$OC1$+$OC2$+$OC3$+OPC, EC = $EC1$+$EC2$+$EC3$-OPC, where

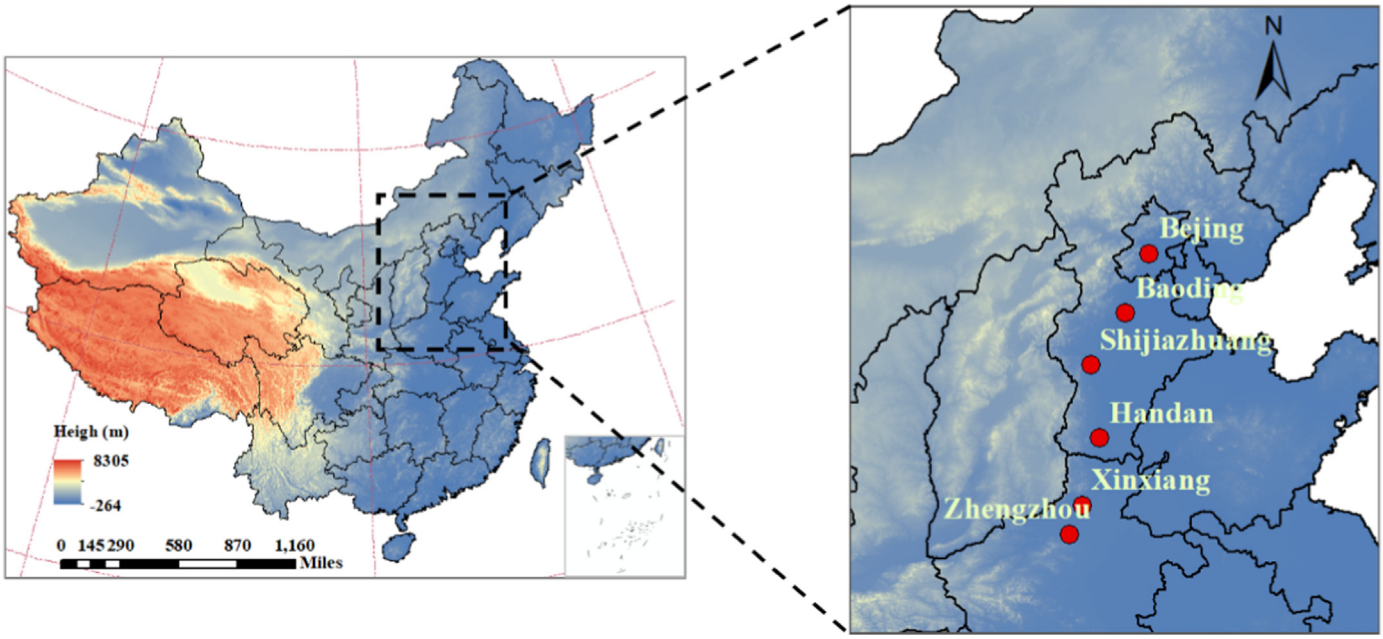

Fig. 1. Geographical location map of six sampling sites in North China.

OPC is the optically pyrolyzed *OC*. More details can be found in Chow et al. (2015).

Secondary organic carbon (SOC) was estimated using the EC-tracer method, which assumes that primary organic carbon (POC) and EC have the same sources with good correlations (Liu et al., 2019; Castro et al., 1999).

$$SOC = OC - POC \tag{1}$$

$$POC = EC \times (OC/EC)_{pri} \tag{2}$$

where OC is the measured ambient OC. The $(OC/EC)_{pri}$ was calculated using the 20th percentile for the lowest OC/EC value (Shao et al., 2018; Lim and Turpin, 2002).

2.4. Potential sources contribution function analysis

By using PSCF, we analyzed backward trajectories of OC and EC mass concentrations at the six sampling sites; meteorological data were downloaded from the NOAA website (ftp://arlftp.arlhq.noaa.gov/pub/archives/gdas1). In previous studies (Zhang et al., 2013; Liu et al., 2019), 48 h simulations were more frequently conducted on potential source analysis; we chose 48 h as the simulation time due to the lifetime of carbonaceous constituents as well as the potential for short-range transmission around the BTH region (Gao et al., 2015; Ji et al., 2019). The simulation start time was 00:00 (Beijing time 08:00), at a height of 500 m above the ground and from 74 to 135°W and 28–58°N, with a 0.5 ° × 0.5 ° resolution. The calculations of the *PSCF* model are as follows:

$$PSCF_{ij} = M_{ij}/N_{ij} \tag{3}$$

where the M_{ij} and N_{ij} represent the number of endpoints that exceed the threshold criterion in the *ij*th cell and the total number of endpoints that fall in the *ij*th cell, respectively. To reduce the uncertainty of N_{ij}, a weighted function W_{ij} was provided as follows:

$$W_{ij} = \begin{cases} 1.00 & 3N_{ave} < N_{ij} \\ 0.7 & 1.5N_{ave} < N_{ij} \le 3N_{ave} \\ 0.42 & N_{ave} < N_{ij} \le 1.5N_{ave} \\ 0.17 & N_{ij} \le N_{ave} \end{cases} \tag{4}$$

where N_{ave} is the average number of endpoints in each cell. The trajectories associated with the daily ambient pollutant concentrations were prepared for the *PSCF* analysis; more details on *PSCF* can be found in Shao et al. (2018).

2.5. Calculation of the light-absorption coefficient (b_{abs})

To obtain the light-absorption coefficient ($b_{abs(\lambda)}$), we first calculated the attenuation (ATN_λ) of the aerosol deposited on the filter. To account for filter matrix artifacts, the ATN_λ values were corrected for the particle light-absorption optical depth (τ) using regression equations established by (Chen et al., 2015):

$$ATN_\lambda = ln(\frac{FT_{\lambda,f}}{FT_{\lambda,i}}) \tag{5}$$

where $FT_{\lambda,f}$ and $FT_{\lambda,i}$ represent the final and initial filter transmittances at each wavelength, respectively.

The procedure described in Chen et al. (2015) suggested that the EC2 step (740 °C in a 98% He/2% O_2 atmosphere) based on the IMPROVE_A protocol is exclusively EC in diesel soot samples with negligible brown BrC and POC; with this assumption, the ATN_λ values from all 1 s measurements at the EC2 step for diesel exhaust samples were retrieved. Simultaneously, the multiwavelength τ was calculated from a mass absorption efficiency (*MAE*) of 7.4 m^2g^{-1} at 635 nm (Chen et al., 2015) and multiplied by the temporal variation in the EC concentration at 1 s at the EC2 step. Finally, at each wavelength, the instrument-specific relationships between ATN_λ and τ were calculated as follows:

$$\tau = \alpha_\lambda ATN_\lambda^2 + \beta_\lambda ATN_\lambda \tag{6}$$

where α_λ and β_λ are coefficients that consider the wavelength-

specific multiple scattering and loading effects from Chen et al. (2015). These τ-*ATN* relationships should apply to any sample, regardless of the nature of the light-absorbing material. τ is the optical depth measuring only the light absorption specific to this study (Chen et al., 2015). The light-absorption coefficient (b_{abs}) at each wavelength was then calculated as follows:

$$b_{abs(\lambda)} = \tau \times \frac{A}{V} \quad (7)$$

where *A* and *V* indicate the filter area (cm^2) and sampling volume (m^3), respectively. Additionally:

$$\tau = q_{BC} \times \lambda^{-AAE_{BC}} + q_{BrC} \times \lambda^{-AAE_{BrC}} \quad (8)$$

$$\tau \times \lambda = q_{BC} + q_{BrC} \times \lambda^{(1-AAE_{BrC})} \quad (9)$$

where *AAE* represents the absorption Ångström exponent, and BC is wavelength-independent; assuming $AAE_{BC} = 1$. The effective AAE_{BrC} value was simulated using Eq. (9) with the lowest mean squared error which ranges 1.5–15. Then, it was put into Eq. (8) to separate BrC from BC. τ was wavelength-dependent which could be calculated at each λ. Previous studies indicate that BrC shows strong light absorption near the UV wavelength, and the contribution of BrC at 405 nm is more significant (Andreae and Gelencser, 2006); thus, we used 405 nm as the example wavelength in this study.

3. Results and discussion

3.1. Seasonal and spatial variations of the $PM_{2.5}$ concentrations at the six sampling sites

Fig. 2 shows the time series of the $PM_{2.5}$ concentrations at the six sampling sites, which were consistent with nearby simultaneous national monitoring site data. When excluding the BJ site, the seasonal variations exhibited similarities among the five sampling sites. Seasonal differences in $PM_{2.5}$ were obvious in North China, especially during the heating period. This suggests clear $PM_{2.5}$ pollution characteristics with regional similarities and complexities in these cities alongside the transmission corridor at the eastern foot of the Taihang Mountains. In addition to the internal cause of the change in the emission intensity, favorable meteorological conditions can also influence the $PM_{2.5}$ concentrations by diffusion (Ding et al., 2019). Time series of meteorological conditions in BJ are shown in Fig. 2(b); $PM_{2.5}$ shows negative correlations with wind speed and a positive correlation with humidity. The average wind speed in the 2017–2018 winter was 2.0 m/s, which was higher than the 1.50 m/s record in autumn and the 0.88 m/s record in BJ winter (2016). The seasonal trend of $PM_{2.5}$ in BJ being opposite that of the other five cities can partially be attributed to the stronger winds for favorable diffusion conditions in the 2017–2018 winter (Zhang et al., 2019).

The seasonal average $PM_{2.5}$ concentrations were 74.2 ± 55.2 and 47.5 ± 49.5 μg/m^3 in the BJ autumn and winter, respectively. In autumn, the $PM_{2.5}$ concentrations in BD, SJZ, and HD were 1.3, 1.3, and 1.1 times, higher than that in BJ, respectively. In contrast, the $PM_{2.5}$ concentrations in XX and ZZ were both slightly lower than those in BJ. In winter, the average $PM_{2.5}$ concentrations in the other five cities were 2.2–2.7 times higher than those in BJ, with the highest to lowest $PM_{2.5}$ concentrations as follows: BD > SJZ > HD > XX > ZZ > BJ. This indicates the complexity of regional air pollution in North China and shows that $PM_{2.5}$ pollution remains a tough challenge compared with the guidelines set by the National Air Quality Standard grade- II (24 h average: 75 μg/m^3; annual average: 35 μg/m^3). The spatial variations of the average

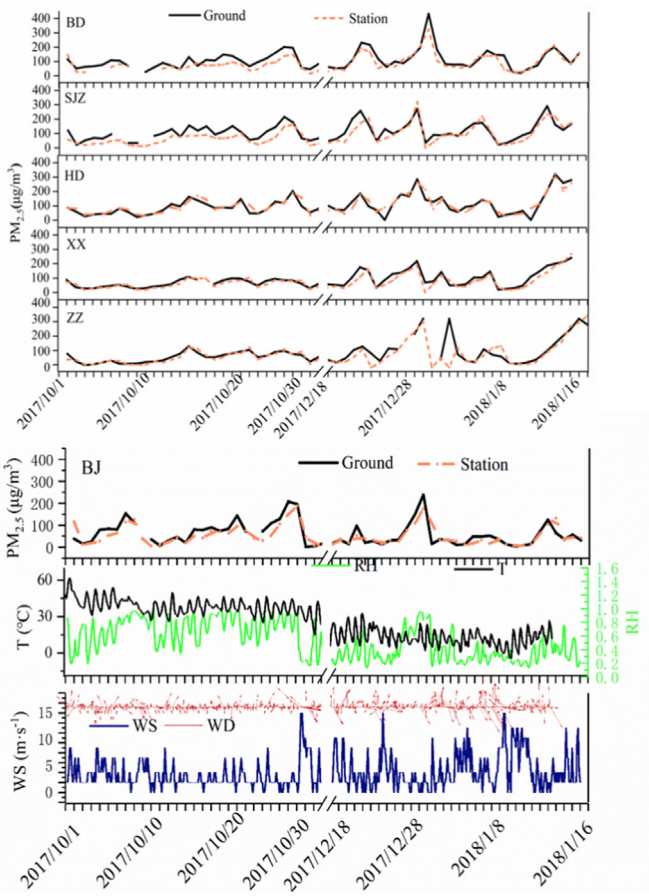

Fig. 2. (a) Time series of ground- and station-based mass concentration of $PM_{2.5}$ at sampling sites (BD, SJZ, HD, XX and ZZ). **(b)** Time series of meteorological variables and $PM_{2.5}$ mass concentration and the meteorological conditions in Beijing 2017–2018.

$PM_{2.5}$ concentrations during the sampling periods show a general decreasing trend from north to south among the six sampling sites. Observations from the time series of the $PM_{2.5}$ peak concentrations show a synchronous pollution process in both autumn and winter due to the impact of regional pollution transportation. In sum, the spatiotemporal variations reveal the regional complexity and interactions of air pollution among these six cities in North China, since they are influenced by the same large-scale weather systems on most occasions.

Table 1 shows a summary of the seasonal $PM_{2.5}$ concentrations in BJ from 2013 to 2017. The observations show a significant reduction in $PM_{2.5}$ pollution during recent years compared with previous studies. The seasonal average $PM_{2.5}$ concentration during the BJ winter decreased by 54% from 2013 to 2017, while, in autumn, the average concentration decreased by 46% from 2014 to 2017 (Gao et al., 2018). This notable decline was mainly caused by the enforced implementation of the APPCAP and the favorable meteorological conditions for diffusion in the BJ winter. To fulfill the specific requirements of the APPCAP, BJ and its surrounding areas have made considerable efforts to diminish emissions from coal combustion, vehicles, industrial sources and biomass burning (Cheng et al., 2019).

In addition, compared to previous studies (Table S2), the results in this study also show similar reductions in the average $PM_{2.5}$ concentrations in BD, SJ (Chen et al., 2017), HD (Meng et al., 2016), XX, and ZZ (Wang et al., 2017) during 2013–2017. The seasonal average $PM_{2.5}$ concentrations in the autumn and winter of 2017

Table 1
Seasonal average concentrations of $PM_{2.5}$ and its carbonaceous components at Beijing during 2013–2017.

Year	Season	$PM_{2.5}$(μg/m^3)	OC(μg/m^3)	EC(μg/m^3)	OC/EC	References
2013	Autumn	–	17.4	2.6	–	(Ji et al., 2014; Zheng et al., 2015)
	Winter	161.77	25.8	4.0	4.99	
2014	Autumn	139.34	32.78	7.8	3.00	Gao et al. (2018)
	Winter	150	48.21	8.92	4.38	
2015	Autumn	109.387	14.1	1.2	7.3	Zhang et al. (2019)
	Winter	103.9	26.9	1.0	7.5	
2016	Autumn	79.9	15.35	5.27	–	Shao et al. (2018)
	Winter	148.69	41.25	11.02	3.21–3.9	
2017	Autumn	74.2	9.56	3.63	2.81	This study
	Winter	47.5	10.27	2.90	3.99	

decreased by 51.4% and 58.6% in BD (2014), 40.0% and 49.0% in SJZ (2013), 35.7% and 43.1% in HD (2013), 37.7% and 22.6% in XX (2015), and 68.9% in ZZ (winter 2013), respectively. Emission reduction rates at all sites were higher than the national average (33%) during 2013–2017 (Zhang et al., 2019), illustrating the high level of emissions reduction made by North China, and suggesting the effectiveness of the implementation of APPCAP. Although great reductions in $PM_{2.5}$ concentrations have been achieved, it remains a considerable challenge to reach the national ambient air quality standard (annual average of 35 μg/m^3) while sustaining continuous economic growth, promoting industries, and applying advanced technologies.

3.2. Characteristics of carbonaceous constituents

3.2.1. Seasonal variations in OC and EC

Fig. 3 shows the seasonal variations in OC and EC at six sampling sites. The average OC and EC concentrations in the BJ winter were 10.27 ± 7.31 and 2.90 ± 1.96 μg/m^3, respectively. The highest OC and EC concentrations occurred in the BD winter, which were 3.88 and 4.26 times more severe, respectively, than those in BJ. This was mainly due to the region's energy structure having a high dependence on coal consumption (Gao et al., 2018). The OC and EC concentrations at the other four sampling sites ranged from 13.32 to 34.65 and from 4.42 to 11.66 μg/m^3, respectively. The lowest OC and EC concentrations were observed in BJ, which can be attributed to strict control measurements and favorable meteorological conditions. The average OC and EC concentrations in the BJ autumn were 9.56 ± 5.14 and 3.63 ± 1.95 μg/m^3. The concentrations of OC and EC in the other five cities ranged from 6.87 to 10.44 μg/m^3 and from 3.98 to 5.45 μg/m^3 in autumn, respectively. Compared with the other five sites, BJ showed insignificant seasonal variations due to the strict progressive transition from coal to clean energy; many manufacturing plants in the area were closed or moved to other locations. Although coal combustion still represents an important source in other cities, the substitution of coal with natural gas and electricity has been implemented to different extents and with varying degrees of success in recent years. In short, these cities show different variation characteristics with respect to seasonal OC and EC concentrations. In addition, it should be noted that possible errors introduced by sampling and testing are inevitable. Our measurements can hardly capture the pollution characteristics of carbonaceous constituents in rapidly forming severe haze, so this concern must be addressed using our approach in combination with online data in future investigations.

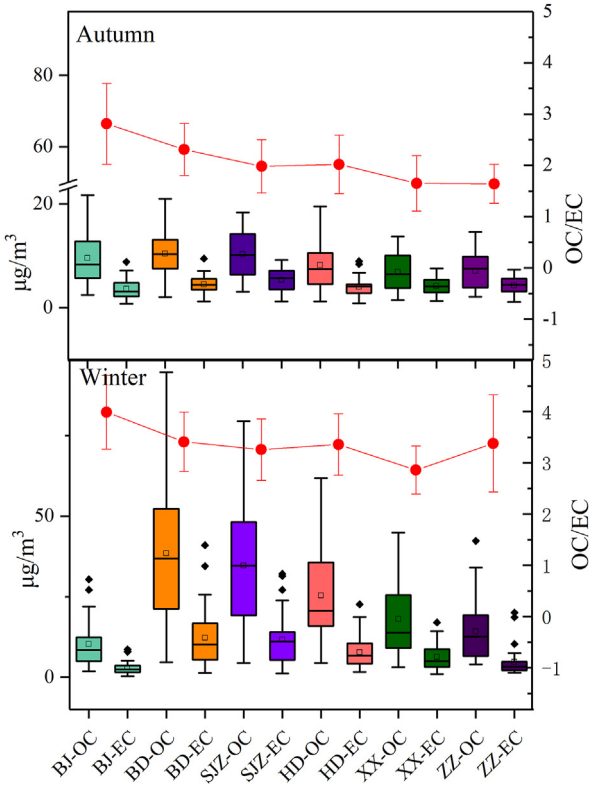

Fig. 3. Seasonal variations of OC and EC at six sampling sites. The mean (hollow circle), median (horizon line in the box), 25th and 75th percentiles (lower and upper end of the box), 10th and 90th percentiles (lower and upper whiskers) are presented. The ⊠represents the average ratio of OC/EC.

To better depict the characteristics of the six sampling sites, we distinguished clean (24 h $PM_{2.5}$ < 75 μg/m^3) and polluted (24 h $PM_{2.5} \geq 75$ μg/m^3) periods during the sampling campaign. In general, OC and EC in the polluted periods were higher than those during the clean periods. Enhancement of POC and SOC was also observed during transitions from clean to polluted days. SOC exhibited a higher relative increase in BJ and ZZ than POC did, and it had a higher relative increase than in the other four cities, suggesting that secondary transformation plays a more important role in the formation of carbonaceous constituents in autumn and winter polluted periods, which agrees well with previous studies (Shao et al., 2018; Ji et al., 2019). These findings indicate that pollution due to secondary carbonaceous aerosols is more prominent because of the larger scales and populations of urban areas as well as the higher vehicle usage in BJ and ZZ. Favorable meteorological conditions for diffusion and lower $PM_{2.5}$ levels facilitate the increased proportion of SOC by photochemical activities (Table S4). POC appeared to be dominant during the polluted periods at the rest of the sites implying a significant contribution from primary emissions. Previous studies have shown a positive correlation among POC, K^+, and levoglucosan, illustrating the important contributions of coal and biomass burning to POC in the studied cities (Xie et al., 2019b).

OC comes from two sources: (1) directly from primary emissions associated with incomplete combustion or solvent use, and (2) is transformation through atmospheric secondary formation and aging. EC is emitted mainly by the incomplete combustion of fossil fuels as well as biomass burning. The concentrations of OC and EC were higher in the winter, mainly as a result of the additional fuel combustion for space heating. The ratio of OC/EC is thought to be a significant parameter indicating the emission source type and characteristics of transformation (Chen et al., 2014). According to previous studies, OC/EC is approximately 4.0 for fossil fuel combustion, ranges from 1.1 to 5.0 for vehicular emissions (Watson et al., 2001), ranges from 8.2 to 12 for residential coal combustion, and ranges from 4.3 to 8.0 for biomass burning (Cao et al., 2005). In this study, the seasonal average OC/EC ranged from 1.64 to 2.81 in autumn and from 2.86 to 3.99 in winter at the six sites, suggesting the diversity of the contributing emission sources in different seasons. The highest OC/EC values were found in the winter at urban sampling sites, suggesting that emission sources were mainly affected by fossil fuel combustion and vehicular emissions. Wang et al. (2017) reported that coal combustion sources accounted for 40% and vehicles accounted for 29% of total emission. Liu et al. (2018) reported that combustion sources accounted for 34% (BC) and 20% (OC) while vehicles accounted for 11% (BC) and 15% (OC) by emission inventory.

Compared with previous studies, concentrations of OC and EC showed a notable change from 2014 to 2017 in BJ. The OC and EC in autumn and winter decreased by 67.62% on average (Table 1), while the seasonal average OC/EC values ranged from 3.00 to 4.38 (2014) and 2.81–3.99 (2017). This significant decrease in OC/EC indicates the effectiveness of replacing coal with clean energy to supply heating and control biomass burning, reflecting the increased contribution of vehicular emissions (Ji et al., 2019). The concentrations of OC and EC, as well as OC/EC, exhibited different degrees of downward trends in BD, SJZ, HD, XX, and ZZ during 2013–2017 (Table S2), revealing that the replacement of coal with natural gas and electricity within these cities was implemented to different degrees and with varying levels of success. This substitution is not only closely correlated with the subjective wills and executive forces for improving local air quality among the governmental authorities of different cities but is also highly influenced by the availability, accessibility, and economic affordability of natural gas.

Changes in OC/EC were also analyzed during the clean and polluted study periods. In general, OC/EC was higher on polluted days due to the strengthening of secondary transformation under meteorological conditions that were unfavorable for diffusion. Nevertheless, lower OC/EC ratios were observed in SJZ, the BD winter, and the HD winter, which can be attributed to the significant role of primary emissions and weaker photochemical activities in polluted periods. Another possible explanation is that SJZ, BD, and HD are all located in the middle of the transmission pathway and are more susceptible to being influenced by long-range transport, regardless of whether northerly or southerly winds pass through the region.

3.2.2. The relationship between OC and EC

Slopes of the regression lines for OC and EC range from 1.98 to 3.49, and the correlations (R^2) range from 0.75 to 0.94 in winter. In autumn, the slope and R^2 are in the ranges of 1.56–3.02 and 0.58–0.86, respectively (Fig. S2). Generally, the slopes of regression lines in winter are higher than those in autumn. A strong R^2 value in winter indicates the strong common emission sources for OC and EC, which could be emitted from various sources, including fuel combustion for space heating and regional transportation of emissions from industrial sources. Wang et al. (2015) reported that combustion sources (13.4–30.6%) and transportation (17.6–30.6%) accounted for significant proportions of OC and EC in BTH region winter. Mao et al. (2020) indicated that vehicular (24.4%) and residential (50%) sources contributed large amounts of BC in the BTH regions in 2017. The seasonal variations of R^2, however, indicate different proportional contributions from various sources across the six cities, revealing discrepancies in their energy structures, as well as their degrees of industrialization and urbanization.

3.3. Potential sources contributing to regional transportation at the six sampling sites

The PSCF results of BJ and BD are shown in Fig. 4, while other results are shown in Fig. S3. The black points represent the locations of the six sampling sites, and the red squares represent the central cities of the PSCF model. The PSCF model was applied to identify the potential sources contributing to emissions that could be attributed to regional transportation at each sampling site.

In BJ autumn, potential sources of OC and EC are mainly transported from Hebei and Henan Provinces through the transmission channel, while the potential sources from Inner Mongolia and Shandong are insignificant. The results differ slightly from those of Ji et al. (2019), partly due to the analysis of two seasons with prevailing southeasterly and southerly winds. In winter, OC originates mainly from the southwestern directions, including northwestern Shandong, central and southeastern Shanxi, and eastern Henan (Ji et al., 2019). In contrast to the dominant sources of OC, local emissions play a significant role in EC contributions.

Potential sources show marked seasonal variations in OC and EC at BD site. In autumn, the important potential sources are located within the transmission channel (SJZ and HD). In winter, the potential sources of OC and EC are mainly from local emissions and parts of Shandong and Shanxi Provinces.

For SJZ, the potential sources of OC and EC are located between the local areas and HD, as well as in select area of Shanxi. In winter, the prominent potential sources mainly originate from the border zone of Hebei and Shanxi Province which agrees well with the results of Xie et al. (2019b).

Potential sources are more dispersed in autumn at HD site. The PSCF results are located along the border zones of Hebei and Henan Provinces. In winter, the potential sources are mainly located near the Hebei-Shandong and Henan-Shanxi Provinces.

Clusters of cities to the northwest of the study area have an influence on the XX site. In autumn, the hotspots are mainly located along the border zone between Henan and Shanxi Provinces and in the central part of Henan. In winter, the results show that clusters of the potential sources of OC and EC are mainly located along the border zone between Henan and Shanxi Provinces, as well as in a small part of northern and central Henan Province.

For ZZ in autumn, potential sources are mainly located along the border zone between Henan and Shanxi as well as in central Henan. Hotspots are observed in the western portion of Shandong Province, the southern portion of Shanxi, and small parts of the adjacent Henan and Anhui Provinces (Liu et al., 2019a). In winter, the potential sources are mainly transported from the northeast and northwest.

Overall, the overlap among the potential sources of the six sampling sites is focused on the border zones of several provinces in North China. Areas with concentrations of heavy industrial manufacturing enterprises remain a substantial challenge for further pollution controls to achieve continuous improvements in the regional air quality in North China.

3.4. Light absorption of carbonaceous constituents

As illustrated in Fig. S2, the average light-absorption coefficients

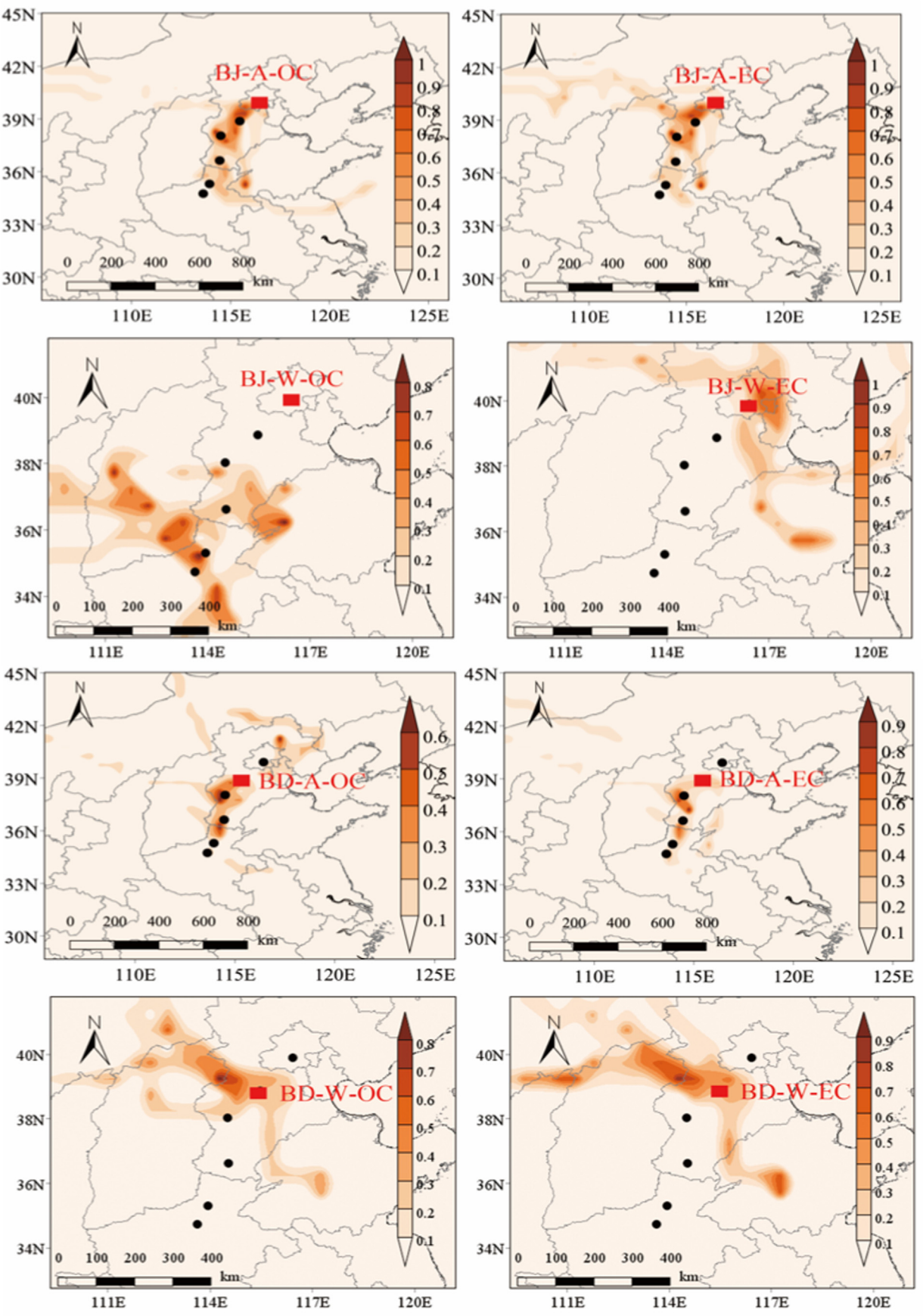

Fig. 4. Seasonal potential sources of EC and OC in BJ and BD by PSCF in the near surface layer (500 m) (A: autumn W: winter).

(b_{abs}) of carbonaceous constituents at six wavelengths (405 nm, 445 nm, 635 nm, 708 nm, 808 nm, and 980 nm) agree very well. Fig. 5 shows that the average light absorption coefficient (b_{abs}) at 405 nm in BJ is 37.74 Mm^{-1} in autumn and 25.21 Mm^{-1} in winter. The light absorption coefficients at the other sampling sites were 1.22–1.58 times higher in autumn and 3.05–3.84 times higher in winter than those in BJ. In general, the dashed lines agree with the histograms, suggesting that BC plays a significant role in the total light absorption of $PM_{2.5}$.

When the collection campaigns are separated into two periods, the b_{abs} values are higher during polluted periods, which agrees with the $PM_{2.5}$ (Table 2). Among the six sampling sites, BJ exhibits the weakest light absorption during the collection periods because of the low carbonaceous constituent content, which is mainly due to the harsh pollution control measurements and favorable diffusion conditions. At most sites, POC is still the driving force of the elevated b_{abs} values in the polluted periods. At BJ and ZZ sites, SOC plays a more significant role in the polluted periods which could attributed to atmospheric chemical transformations (Shao et al., 2018).

3.5. Contributions and absorption Ångström exponent of brown carbon

As seen in Fig. 6, the BrC light absorption contribution exhibits strong seasonality. The light absorption of BrC is higher in winter than in autumn, which is consists well with the results of previous studies (Shen et al., 2017; Yuan et al., 2016). The contributions of BrC accounting for the total $PM_{2.5}$ light absorption in BJ, BD, SJZ, HD, XX, and ZZ at 405 nm were 2.75%, 4.39%, 6.94%, 0.55%, 1.21%, and 3.51%, respectively, in autumn, whereas the contributions increase to approximately 21.22%, 33.26%, 34.71%, 39.09%, 48.58%, and 23.28%, respectively in winter. The enhancement of the BrC light-absorption contribution in winter with the elevated SOC/OC values (Table S4.) at ZZ site suggests that BrC mainly originates from secondary organic aerosols. In contrast, the lower SOC/OC values at the other five sites indicate that the primary organic aerosols are predominant. The ratios of $b_{abs,BrC}/b_{abs,BC}$ in autumn were insignificant, ranging from 0.01 to 0.16, while those in winter averaged 0.27, 0.50, 0.53, 0.64, 0.96, and 0.30 in BJ, BD, SJZ, HD, XX, and ZZ, respectively. In particular, $b_{abs,BrC}$ was comparable to $b_{abs,BC}$ in Xinxiang due to the high local emissions of organic solvents (Liu et al., 2019a).

Yuan et al. (2016) reported that the contributions of BrC in Shenzhen accounted for 11.4% and 6.3% of the light absorption at 405 nm in winter and autumn of 2014, respectively. The contributions of BrC were 19.7% in winter and 17% in autumn at 370 nm in Nanjing (Wang et al., 2018). Yang et al. (2009) also reported that the

Table 2
A summary of average OC, EC, OC/EC, b_{abs} values during clean and polluted periods in autumn (upper gray shade) and winter (down no background) at six sampling sites.

Season	Sites	OC		EC		OC/EC		b_{abs}	
		C	P	C	P	C	P	C	P
Winter	BJ	5.93	11.92	2.64	4.16	2.65	2.85	17.24	46.53
	BD	7.62	12.43	3.21	5.40	2.31	2.32	33.07	62.42
	SJZ	7.27	13.02	3.35	6.84	2.11	1.89	31.78	79.07
	HD	5.83	10.13	3.10	4.82	1.82	2.12	27.16	50.29
	XX	5.03	9.32	3.16	5.55	1.61	1.69	27.34	74.94
	ZZ	5.26	9.79	3.27	5.74	1.60	1.73	21.44	69.91
Autumn	BJ	7.81	23.09	2.26	6.23	3.54	3.79	18.04	57.50
	BD	29.61	42.03	8.12	13.90	3.57	3.35	74.23	111.47
	SJZ	13.70	40.76	3.93	13.92	3.45	3.20	34.66	107.36
	HD	12.17	31.28	3.44	9.74	3.42	3.33	56.82	85.28
	XX	8.45	23.55	2.92	8.28	2.84	2.88	59.02	83.88
	ZZ	9.86	17.34	3.82	5.36	3.17	3.53	55.65	62.76

Note: C is clean periods; P is polluted periods.

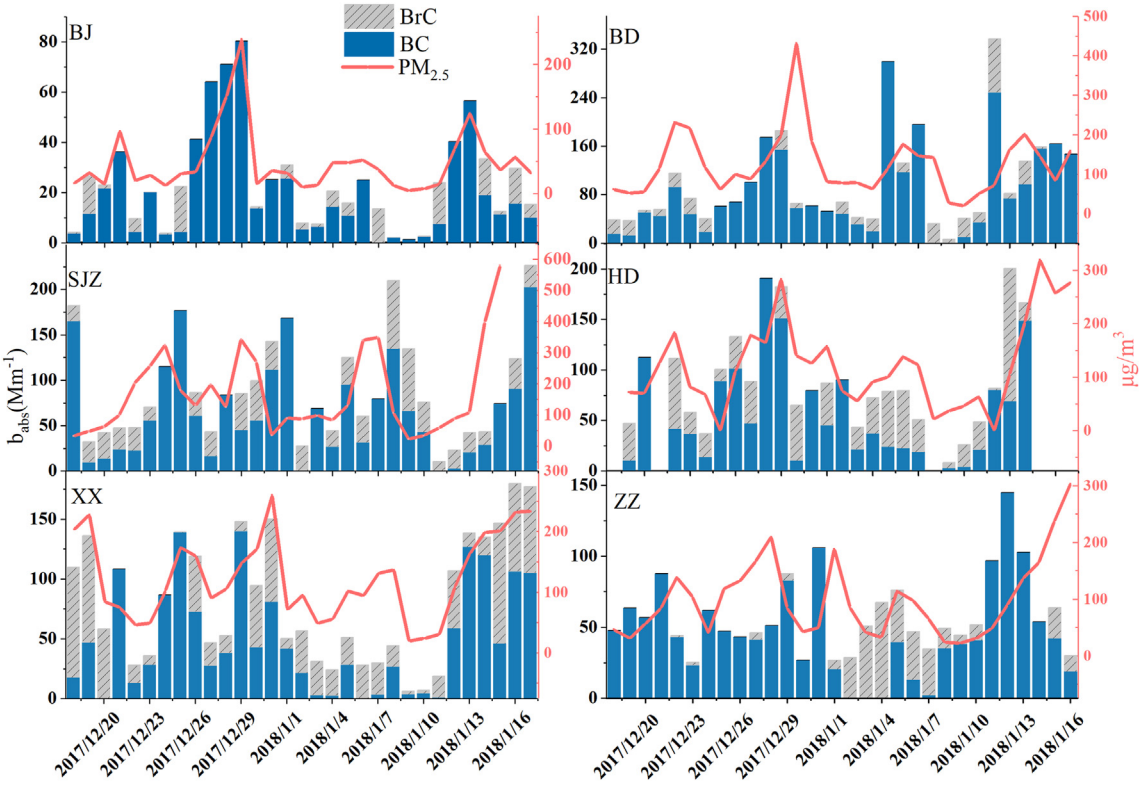

Fig. 5. Time series of $PM_{2.5}$ concentration of and light absorption coefficients of carbonaceous aerosols (405) at six sites.

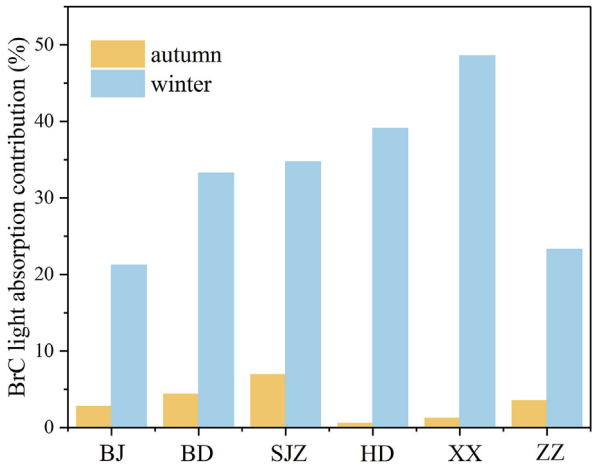

Fig. 6. BrC light absorption contribution in winter and autumn at six sampling sites.

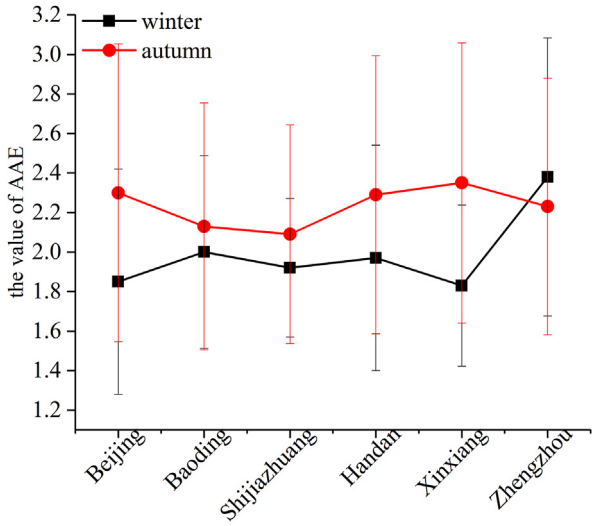

Fig. 7. Characteristics of BrC absorption Ångström exponent at six sampling sites.

contribution of BrC in Xianghe at 370 nm was 30%. Previous studies and different methods show that the overall trend of BrC in the BTH region is higher than that in the YRD and PRD.

Xie et al. (2019a) reported that BrC accounted for 46% of the absorption at 370 nm in BJ winter, which is higher than the contribution of 21.22% at 405 nm determined in this study. This is mainly due to the strong light absorption of BrC in the near-ultraviolet-visible wavelength range of the spectrum and favorable meteorological conditions (Xie et al., 2019a). Sources of BrC are mainly from fossil fuel combustion in winter and biomass burning in autumn; potential sources of OC may also influence the contribution of BrC to the total light absorption.

The average AAE_{BrC} values among the five sampling sites in BJ, BD, SJZ, HD, XX, and ZZ were 2.3, 2.13, 2.09, 2.29, 2.35, and 2.23, respectively, in autumn whereas the averages were 1.85, 2.02, 1.93, 1.98, 1.84, and 2.38 in winter, which is consistent with the results of previous studies (Lei et al., 2019; Lukács et al., 2007). Seasonal discrepancies among all AAE_{BrC} values are indicative of the different sources in different seasons. BrC is a part of OC closely associated with biomass burning and fossil fuel combustion. We summarized the variations in AAE_{BrC} values associated with different emission sources in different methods from relevant references. When AAE_{BrC} is larger than (but close to) 1, BrC originates largely from fossil fuel combustion (Ajtaiet et al., 2015). When AAE_{BrC} ranges from 1 to 3, it mainly originates from incomplete biomass burning (Adam et al., 2020; Martinsson et al., 2015) or wood burning (Ajtaiet et al., 2015); finally, when AAE_{BrC} ranges from 3 to 7, it may transform into secondary BrC after going through the atmospheric aging process (Yan et al., 2018). Overall, according to the range of AAE_{BrC} values in this study, biomass burning and fossil fuels are thought to be the main sources at the six sites in North China. In winter, BrC mainly originated from coal combustion and vehicle exhaust in stable atmospheric conditions (Yan et al., 2017). High AAE_{BrC} in ZZ may be caused by the high local emission of VOCs from solvent sources such as chemical pesticide production, which favors the formation of BrC by atmospheric photochemical reactions (Liu et al., 2019a).

It should be mentioned that many methods exist for segregating the *AAE* to determine their specific sources, while some methods aim to separate BrC from BC using different instruments, which may lead to large differences. Cheng et al. (2016) showed that the AAE_{BrC} was 7.10 in BJ winter, which is higher than the value in this study mainly because they utilized water-soluble organic components as a surrogate for BrC. Xie et al. (2019a) also reported that the *AAE* in BJ winter was 1.58, indicating the important role of BrC in carbonaceous constituents. Previous studies also reported that AAE_{BrC} in Europe was dominated by residual wood burning and traffic in winter, varying between 1.25 and 2 (Favaz et al., 2009; Utry et al., 2014); however, real BrC is more complex in terms of its chemical composition, mixing state, etc. There are correlations between the chemical refractivity and spectral responses of carbonaceous particulate matter (Pöschl, 2003). Previous studies have also demonstrated the wavelength dependency of *AAE* (Pintér et al., 2018; Ajtai et al., 2019). Light-absorption properties measured at 405 nm for $PM_{2.5}$ may be insufficient to well identify sources or aging processes, such as photochemical reactivity during atmospheric transport. Hence, the applicability of the results of the light absorption properties of BrC using the AAE_{BrC} value to reflect real aerosol behavior requires further investigation that necessitates the use of a chemical analyzer.

4. Conclusions

We investigated the variations in characteristics of carbonaceous constituents including their mass concentration and light absorption by collecting multisite observations at six sites in North China from autumn (1–October 30, 2017) to winter (from December 18, 2017 to January 17, 2018). The concentrations of $PM_{2.5}$, OC, and EC at six sites showed seasonally dependent patterns. The decline in the ratios of $PM_{2.5}$ concentrations reflects the large contribution that government policies enacted in North China during 2013–2017.

In polluted periods in both seasons, higher increases in SOC are observed than in POC in BJ and ZZ, suggesting that secondary aerosol pollution plays a significant role in polluted periods. The b_{abs} values are higher in polluted periods with increasing $PM_{2.5}$. BrC accounted for 21.2–48.5% of the total light absorption at six sites in winter. BrC in winter showed enhanced light absorption in response to the increase in primary emissions. The ratios of $b_{abs,BrC}/b_{abs,BC}$ at 405 nm among the six sites ranged from 0.27 to 0.96 in winter. In particularly, BrC was comparable to BC in XX, which deserves further investigation combined with on-line instruments or chemical analyzers (GC-MS, AMS, or others) for more clarity.

Estimating the light absorption contribution of BrC in $PM_{2.5}$ provides a comprehensive understanding of carbonaceous constituents, suggesting that aerosol radiative forcing could be

considerably underestimated if the absorption of BrC were neglected. Our study provides a reference for regionally estimating BrC using a unified method, and the results provided herein indicate that further observations and validations remain necessary and urgent.

Declaration of competing interest

The authors declare that they have no known competing financial interests or personal relationships that could have appeared to influence the work reported in this paper.

Acknowledgements

This work was funded by the National Natural Science Foundation of China (21777008, 51678056, 21377012, and 21177012), the Trail Special Program of Research on the Cause and Control Technology of Air Pollution under the National Key Research and Development Plan of China (2018YFC0213202, 2016YFC0201501), and the National Key Scientific and Technological Project on Formation Mechanism and Control of Heavily Air Pollution (DQGG0209). We thank the editors and anonymous reviewers for their valuable suggestions and comments on improving this paper.

Appendix A. Supplementary data

Supplementary data to this article can be found online at https://doi.org/10.1016/j.envpol.2020.115780.

References

Andreae, M.O., Gelencśer, A., 2006. Black carbon or brown carbon? The nature of light-absorbing carbonaceous aerosols. Atmos. Chem. Phys. 6, 3131–3148.
Ajtai, T., Utry, N., Pintér, M., Major, B., Bozóki, Z., Szabó, G., 2015. A method for segregating the optical absorption properties and the mass concentration of winter time urban aerosol. Atmos. Environ. 122, 313–320.
Ajtai, T., Kiss-Albert, G., Utry, N., Tóth, Á., Hoffer, A., Szabó, G., Bozóki, Z., 2019. Diurnal variation of aethalometer correction factors and optical absorption assessment of nucleation events using multi-wavelength photoacoustic spectroscopy. J. Environ. Sci. 83, 96–109.
Araki, S., Shima, M., Yamamoto, K., 2020. Estimating historical $PM_{2.5}$ exposures for three decades (1987-2016) in Japan using measurements of associated air pollutants and land use regression. Environ. Pollut. 263.
Bond, T.C., Doherty, S.J., Fahey, D.W., Forster, P.M., Berntsen, T., DeAngelo, B.J., Flanner, M.G., Ghan, S., Kärcher, B., Koch, D., Kinne, S., Kondo, Y., Quinn, P.K., Sarofim, M.C., Schultz, M.G., Schulz, M., Venkataraman, C., Zhang, H., Zhang, S., Bellouin, N., Guttikunda, S.K., Hopke, P.K., Jacobson, M.Z., Kaiser, J.W., Klimont, Z., Lohmann, U., Schwarz, J.P., Shindell, D., Storelvmo, T., Warren, S.G., Zender, C.S., 2013. Bounding the role of black carbon in the climate system: a scientific assessment. J. Geophys. Res. Atmos. 118 (11), 5380–5552.
Cao, G., Zhang, X., Wang, D., Zheng, F., 2005. Emission inventory of biomass burning in Chinese mainland. China Environ. Sci. 25 (4), 389–393.
Castro, L., Pio, C., Harrison, R., Smith, D., 1999. Carbonaceous aerosol in urban and rural European atmospheres: estimation of secondary organic carbon concentrations. Atmos. Environ. 33 (17), 2771–2781.
Cavalli, F., Viana, M., Yttri, K.E., Genberg, J., Putaud, J.P., 2010. Toward a standardised thermal-optical protocol for measuring atmospheric organic and elemental carbon: the EUSAAR protocol. Atmos. Meas Tech 3, 79–89.
Chen, F., Zhang, X., Zhu, X., Zhang, H., Gao, J., Hopke, P.K., 2017. Chemical characteristics of $PM_{2.5}$ during a 2016 winter haze episode in Shijiazhuang, China. Aerosol Air Qual. Res. 17 (2), 368–380.
Chen, L.W.A., Chow, J.C., Wang, X.L., Robles, J.A., Sumlin, B.J., Lowenthal, D.H., Zimmermann, R., Watson, J.G., 2015. Multi-wavelength optical measurement to enhance thermal/optical analysis for carbonaceous aerosol. Atmos. Meas Tech. 8 (1), 451–461.
Chen, Y., Xie, S., Luo, B., Zhai, C., 2014. Characteristics and origins of carbonaceous aerosol in the Sichuan Basin, China. Atmos. Environ. 94, 215–223.
Cheng, J., Su, J., Cui, T., Li, X., Dong, X., Sun, F., Yang, Y., Tong, D., Zheng, Y., Li, Y., Li, J., Zhang, Q., He, K., 2019. Dominant role of emission reduction in $PM_{2.5}$ air quality improvement in Beijing during 2013–2017: a model-based decomposition analysis. Atmos. Chem. Phys. 19 (9), 6125–6146.
Cheng, Y., He, K., Du, Z.y., Engling, G., Liu, J., Ma, Y., Zheng, M., Weber, R.J., 2016. The characteristics of brown carbon aerosol during winter in Beijing. Atmos. Environ. 127, 355–364.
Chow, J.C., Wang, X., Sumlin, B.J., Gronstal, S.B., Chen, L.W.A., Trimble, D.L., Watson, J.G., Kohl, S.D., Mayorga, S.R., Riggio, G., Hurbain, P.R., Johnson, M., Zimmermann, R., 2015. Optical calibration and equivalence of a multiwavelength thermal/optical carbon analyzer. Aerosol Air Qual. Res. 15 (4), 1145–1159.
Ding, D., Xing, J., Wang, S., Liu, K., Hao, J., 2019. Estimated contributions of emissions controls, meteorological factors, population growth, and changes in baseline mortality to reductions in ambient $PM_{2.5}$ and $PM_{2.5}$-related mortality in China, 2013–2017. Environ. Health Perspect. 127 (6).
Favez, O., Cachier, H., Sciare, J., Sarda-Estève, R., Martinon, L., 2009. Evidence for a significant contribution of wood burning aerosols to PM2.5 during the winter season in Paris, France. Atmos. Environ. 43 (22–23), 3640–3644.
Feng, Y., Ramanathan, V., Kotamarthi, V.R., 2013. Brown carbon: a significant atmospheric absorber of solar radiation? Atmos. Chem. Phys. 13 (1), 8608–8621.
Galvao, M.F.D., Alves, N.D., Ferreira, P.A., Caumo, S., Vasconcellos, P.D., Artaxo, P., Hacon, S.D., Roubicek, D.A., de Medeiros, S.R.B., 2018. Biomass burning particles in the Brazilian Amazon region: mutagenic effects of nitro and oxy-PAHs and assessment of health risks. Environ. Pollut. 233, 960e970.
Gao, J., Wang, K., Wang, Y., Liu, S., Zhu, C., Hao, J., Liu, H., Hua, S., Tian, H., 2018. Temporal-spatial characteristics and source apportionment of $PM_{2.5}$ as well as its associated chemical species in the Beijing-Tianjin-Hebei region of China. Environ. Pollut. 233, 714–724.
Ji, D., Gao, M., Maenhaut, W., He, J., Wu, C., Cheng, L., Gao, W., Sun, Y., Sun, J., Xin, J., Wang, L., Wang, Y., 2019. The carbonaceous aerosol levels still remain a challenge in the Beijing-Tianjin-Hebei region of China: Insights from continuous high temporal resolution measurements in multiple cities. Environ. Int. 126, 171–183.
Ji, D., Li, L., Wang, Y., Zhang, J., Cheng, M., Sun, Y., Liu, Z., Wang, L., Tang, G., Hu, B., Chao, N., Wen, T., Miao, H., 2014. The heaviest particulate air-pollution episodes occurred in northern China in January, 2013: Insights gained from observation. Atmos. Environ. 92, 546–556.
Koch, D., Bond, T.C., Streets, D., Unger, N., van der Werf, G.R., 2007. Global impacts of aerosols from particular source regions and sectors. J. Geophys. Res. Atmos. 112 (D2).
Lei, Y., Shen, Z., Zhang, T., Lu, D., Zeng, Y., Zhang, Q., Xu, H., Bei, N., Wang, X., Cao, J., 2019. High time resolution observation of $PM_{2.5}$ Brown carbon over Xi'an in northwestern China: seasonal variation and source apportionment. Chemosphere 237, 124530.
Li, Z., Tan, H., Zheng, J., Liu, L., Qin, Y., Wang, N., Li, F., Li, Y., Cai, M., Ma, Y., Chan, C.K., 2019. Light absorption properties and potential sources of particulate brown carbon in the Pearl River Delta region of China. Atmos. Chem. Phys. 19 (18), 11669–11685.
Lim, H., Turpin, B., 2002. Origins of primary and secondary organic aerosol in Atlanta supersite experiment. Environ. Sci. Technol. 36 (21), 4489–4496.
Liu, H., Tian, H., Zhang, K., Liu, S., Cheng, K., Yin, S., Liu, Y., Liu, X., Wu, Y., Liu, W., Bai, X., Wang, Y., Shao, P., Luo, L., Lin, S., Chen, J., Liu, X., 2019a. Seasonal variation, formation mechanisms and potential sources of $PM_{2.5}$ in two typical cities in the Central Plains Urban Agglomeration, China. Sci. Total Environ. 657, 657–670.
Liu, S., Zhu, C., Tian, H., Wang, Y., Zhang, K., Wu, B., Liu, X., Hao, Y., Liu, W., Bai, X., Lin, S., Wu, Y., Shao, P., Liu, H., 2019b. Spatiotemporal variations of ambient concentrations of Trace Elements in a highly polluted region of China. J. Geophys. Res. Atmos. 124 (7), 4186–4202.
Lukács, H., Gelencsér, A., Hammer, S., Puxbaum, H., Pio, C., Legrand, M., Kasper-Giebl, A., Handler, M., Limbeck, A., Simpson, D., Preunkert, S., 2007. Seasonal trends and possible sources of brown carbon based on 2-year aerosol measurements at six sites in Europe. J. Geophys. Res. Atmos. 112 (D23).
Martinsson, J., Eriksson, A.C., Nielsen, I.E., Malmborg, V.B., Ahlberg, E., Andersen, C., Lindgren, R., Nystrom, R., Nordin, E.Z., Brune, W.H., Svenningsson, B., Swietlicki, E., Boman, C., Pagels, J.H., 2015. Impacts of combustion conditions and photochemical processing on the light absorption of biomass combustion aerosol. Environ. Sci. Technol. 49 (24), 14663–14671.
Mao, Y.H., Zhao, X., Liao, H., Zhao, D., Tian, P., Henze, D.K., Cao, H., Zhang, L., Li, J., Li, J., Ran, L., Zhang, Q., 2020. Sources of black carbon during severe haze events in the Beijing-Tianjin-Hebei region using the adjoint method. Sci. Total Environ. 740, 140149.
Mbengue, S., Serfozo, N., Schwarz, J., Zikova, N., Smejkalova, A.H., Holoubek, I., 2020. Characterization of equivalent black carbon at a regional background site in central Europe: variability and source apportionment. Environ. Pollut.
Meng, C., Wang, L., Zhang, F., Wei, Z., Ma, S., Ma, X., Yang, J., 2016. Characteristics of concentrations and water-soluble inorganic ions in $PM_{2.5}$ in Handan City, Hebei province, China. Atmos. Res. 171, 133–146.
Menon, S., Hansen, J., Nazarenko, L., Luo, Y., 2002. Climate effects of black carbon aerosols in China and India. Science 297 (5590), 2250–2253.
Pöschl, U., 2003. Aerosol particle analysis: challenges and progress. Anal. Bioanal. Chem. 375 (1), 30–32.
Petaja, T., Jarvi, L., Kerminen, V., Ding, A., Sun, J., Nie, W., Kujansuu, J., Virkkula, A., Yang, X., Fu, C., Zilitivich, S., Kulmala, M., 2016. Enhanced air pollution via aerosol-boundary layer feedback in China. Sci. Rep. 6 (1), 18998-18998.
Pintér, M., Ajtai, T., Kiss-Albert, G., Kiss, D., Utry, N., Janovszky, P., Palásti, D., Smausz, T., Kohut, A., Hopp, B., Galbács, G., Kukovecz, Á., Kónya, Z., Szabó, G., Bozóki, Z., 2018. Thermo-optical properties of residential coals and combustion aerosols. Atmos. Environ. 178, 118–128. https://doi.org/10.1016/j.atmosenv.2018.01.036.
Sarkar, C., Venkataraman, C., Yadav, S., Phuleria, H.C., Chatterjee, A., 2019. Origin and properties of soluble brown carbon in freshly emitted and aged ambient aerosols over an urban site in India. Environ. Pollut. 254, 113077.

Shao, P., Tian, H., Sun, Y., Liu, H., Wu, B., Liu, S., Liu, X., Wu, Y., Liang, W., Wang, Y., Gao, J., Xue, Y., Bai, X., Liu, W., Lin, S., Hu, G., 2018. Characterizing remarkable changes of severe haze events and chemical compositions in multi-size airborne particles (PM_1, $PM_{2.5}$ and PM_{10}) from January 2013 to 2016–2017 winter in Beijing, China. Atmos. Environ. 189, 133–144.

Shen, Z., Zhang, Q., Cao, J., Zhang, L., Lei, Y., Huang, Y., Huang, R., Gao, J., Zhao, Z., Zhu, C., Yin, X., Zheng, C., Xu, H., Liu, S., 2017. Optical properties and possible sources of brown carbon in $PM_{2.5}$ over Xi'an, China. Atmos. Environ. 150, 322–330.

Tian, H., Wang, Y., Xue, Z., Qu, Y., Chai, F., Hao, J., 2011. Atmospheric emissions estimation of Hg, As, and Se from coal-fired power plants in China, 2007. Sci. Total Environ. 409 (16), 3078–3081.

Tian, J., Wang, Q., Ni, H., Wang, M., Zhou, Y., Han, Y., Shen, Z., Pongpiachan, S., Zhang, N., Zhao, Z., Zhang, Q., Zhang, Y., Long, X., Cao, J., 2019. Emission characteristics of primary Brown carbon absorption from biomass and coal burning: development of an optical emission inventory for China. J. Geophys. Res. Atmos.

Utry, N., Ajtai, T., Filep, Á., Pintér, M., Török, Z., Bozóki, Z., Szabó, G., 2014. Correlations between absorption Angström exponent (AAE) of wintertime ambient urban aerosol and its physical and chemical properties. Atmos. Environ. 91, 52–59.

Wang, J., Nie, W., Cheng, Y., Shen, Y., Chi, X., Wang, J., Huang, X., Xie, Y., Sun, P., Xu, Z., Qi, X., Su, H., Ding, A., 2018. Light absorption of brown carbon in eastern China based on 3-year multi-wavelength aerosol optical property observations and an improved absorption Ångström exponent segregation method. Atmos. Chem. Phys. 18 (12), 9061–9074.

Wang, L., Wei, Z., Wei, W., Fu, J.S., Meng, C., Ma, S., 2015. Source apportionment of PM $_{2.5}$ in top polluted cities in Hebei, China using the CMAQ model. Atmos. Environ. 122, 723–736.

Wang, Q., Jiang, N., Yin, S., Li, X., Yu, F., Guo, Y., Zhang, R., 2017. Carbonaceous species in $PM_{2.5}$ and PM_{10} in urban area of Zhengzhou in China: seasonal variations and source apportionment. Atmos. Res. 191, 1–11.

Watson, J.G., Chow, J.C., Houck, J.E., 2001. $PM_{2.5}$ chemical source profiles for vehicle exhaust, vegetative burning, geological material, and coal burning in Northwestern Colorado during 1995. Chemospere 43 (8), 1141–1151.

Who, 2018. World Health Statistics 2018: Monitoring Health for the SDGs, Sustainable Development Goals.

Wiedensohler, A., Cheng, Y., Nowak, A., Wehner, B., Achtert, P., Berghof, M., Birmili, W., Wu, Z., Hu, M., Zhu, T., Takegawa, N., Kita, K., Kondo, Y., Lou, S., Hofzumahaus, A., Holland, F., Wahner, A., Gunthe, S.S., Rose, D., Su, H., Poschl, U., 2009. Rapid aerosol particle growth and increase of cloud condensation nucleus activity by secondary aerosol formation and condensation: a case study for regional air pollution in northeastern China. J.Geophs. Res. 114, D00G08.

Wu, C., Huang, X.H.H., Ng, W.M., Griffith, S.M., Yu, J.Z., 2016. Inter-comparison of NIOSH and IMPROVE protocols for OC and EC determination: implications for inter-protocol data conversion. Atmospheric Measurement Techniques 9 (9), 4547–4560.

Xie, C., Xu, W., Wang, J., Wang, Q., Liu, D., Tang, G., Chen, P., Du, W., Zhao, J., Zhang, Y., Zhou, W., Han, T., Bian, Q., Li, J., Fu, P., Wang, Z., Ge, X., Allan, J., Coe, H., Sun, Y., 2019a. Vertical characterization of aerosol optical properties and brown carbon in winter in urban Beijing, China. Atmos. Chem. Phys. 19 (1), 165–179.

Xie, Y., Liu, Z., Wen, T., Huang, X., Liu, J., Tang, G., Yang, Y., Li, X., Shen, R., Hu, B., Wang, Y., 2019b. Characteristics of chemical composition and seasonal variations of $PM_{2.5}$ in Shijiazhuang, China: impact of primary emissions and secondary formation. Sci. Total Environ. 677, 215–229.

Yan, C., Zheng, M., Bosch, C., Andersson, A., Desyaterik, Y., Sullivan, A.P., Collett, J.L., Zhao, B., Wang, S., He, K., Gustafsson, O., 2017. Important fossil source contribution to brown carbon in Beijing during winter. Sci. Rep. 7, 43182.

Yan, J., Wang, X., Gong, P., Wang, C., Cong, Z., 2018. Review of brown carbon aerosols: recent progress and perspectives. Sci. Total Environ. 634, 1475–1485.

Yang, M., Howell, S.G., Zhuang, J., Huebert, B.J., 2009. Attribution of aerosol light absorption to blackcarbon, brown carbon, and dust in China – interpretations of atmospheric measurements during EAST-AIRE. Atmos. Chem. Phys. 9, 2035–2050.

Yttri, K.E., Simpson, D., Bergström, R., Kiss, G., Szidat, S., Ceburnis, D., Eckhardt, S., Hueglin, C., Nøjgaard, J.K., Perrino, C., Pisso, I., Prevot, A.S.H., Putaud, J.-P., Spindler, G., Vana, M., Zhang, Y.-L., Aas, W., 2019. The EMEP Intensive Measurement Period campaign, 2008–2009: characterizing carbonaceous aerosol at nine rural sites in Europe. Atmos. Chem. Phys. 19 (6), 4211–4233.

Yuan, J., Huang, X., Cao, L., Cui, J., Zhu, Q., Huang, C., Lan, Z., He, L., 2016. Light absorption of brown carbon aerosol in the PRD region of China. Atmos. Chem. Phys. 16 (3), 1433–1443.

Zhang, Q., Zheng, Y., Tong, D., Shao, M., Wang, S., Zhang, Y., Xu, X., Wang, J., He, H., Liu, W., Ding, Y., Lei, Y., Li, J., Wang, Z., Zhang, X., Wang, Y., Cheng, J., Liu, Y., Shi, Q., Yan, L., Geng, G., Hong, C., Li, M., Liu, F., Zheng, B., Cao, J., Ding, A., Gao, J., Fu, Q., Huo, J., Liu, B., Liu, Z., Yang, F., He, K., Hao, J., 2019. Drivers of improved $PM_{2.5}$ air quality in China from 2013 to 2017. P. Natl. Acad. Sci. USA 116 (49), 24463–24469.

Zhao, P., Dong, F., Yang, Y., He, D., Zhao, X., Zhang, W., Yao, Q., Liu, H., 2013. Characteristics of carbonaceous aerosol in the region of beijing, Tianjin, and Hebei, China. Atmos. Environ. 71, 389–398.

Zhao, R., Lee, A.K.Y., Huang, L., Li, X., Yang, F., Abbatt, J.P.D., 2015. Photochemical processing of aqueous atmospheric brown carbon. Atmos. Chem. Phys. 15 (11), 6087–6100.

Zhao, Z., Cao, J., Chow, J.C., Watson, J.G., Chen, A.L.W., Wang, X., Wang, Q., Tian, J., Shen, Z., Zhu, C., Liu, S., Tao, J., Ye, Z., Zhang, T., Zhou, J., Tian, R., 2019. Multi-wavelength light absorption of black and brown carbon at a high-altitude site on the Southeastern margin of the Tibetan Plateau, China. Atmos. Environ. 212, 54–64.

Zheng, G., Duan, F., Su, H., Ma, Y., Cheng, Y., Zheng, B., Zhang, Q., Huang, T., Kimoto, T., Chang, D., Pöschl, U., Cheng, Y., He, K., 2015. Exploring the severe winter haze in Beijing: the impact of synoptic weather, regional transport and heterogeneous reactions. Atmos. Chem. Phys. 15, 2969–2983.